Design of ferromagnetic shape memory alloy composite made of Fe and TiNi particles

S. Gururaja[a] and M. Taya[b]
Center of Intelligent Materials and Systems (CIMS), Department of Mechanical Engineering, University of Washington, Box 352600 Seattle, Washington 98195-2600, USA

Y. S. Kang
Department of Material Processing, Tohoku University, Sendai, Japan

(Received 13 March 2007; accepted 14 July 2007)

Ferromagnetic shape memory alloy (FSMA) particulate composites have been processed by spark plasma sintering with varying weight fractions of NiTi (51 at. % Ni) and Fe powders. An assortment of experimental processing conditions such as temperature, pressure, duration of sintering, and heating rate has been chosen to characterize the relative density and superelasticity behavior of the said FSMA composite. The effective magnetic properties of these processed composites have also been experimentally estimated using vibrating sample magnetometry. An attempt at predicting the effective magnetic properties of the FSMA composite based on Eshelby's inhomogeneous inclusion method in conjunction with Mori-Tanaka's mean-field theory for larger concentrations of the ferromagnetic phase has also been presented in this study. The analytical model results thus obtained are compared with experimental data resulting in reasonably good agreement. © *2007 American Institute of Physics*. [DOI: 10.1063/1.2775289]

INTRODUCTION

Ferromagnetic shape memory alloys (FSMAs) have attracted strong attention from the material science community in particular and actuator designers in general mainly due to their fast response and large strain capabilities. Popular FSMAs that have been extensively studied include NiMnGa (Refs. 1–5) and FePd (Refs. 6–8) systems. There are three mechanisms of actuation associated with FSMAs under magnetic field, namely, (i) magnetic-field-induced phase transformation, (ii) martensite variant rearrangement, and (iii) hybrid mechanism.[9] The first two mechanisms are operative under constant magnetic field, while the third mechanism is based on gradient magnetic field.

An earlier study by Kato *et al.*,[6] which was based on thermodynamics, made a preliminary estimate of the magnetic energy necessary to induce a phase transformation in FSMAs. The general conclusion was that a large magnetic (H) field was required for the phase change to take place for both NiMnGa and FePd systems. Therefore, the first mechanism was deemed unsuitable for use in designing compact actuators which may need a small and portable electromagnet system as a driving unit.

The second mechanism involves inducing the strain in a FSMA with 100% martensite phase and subjecting it to a *constant H* field which acts on the magnetic moments in magnetic domains that exist in the martensite phase so as to rotate them along the easy axis, i.e., c axis in the case of NiMnGa and FePd systems. Even though the strain induced by the second mechanism is very large, the corresponding stress remains as modest as several megapascals under modest applied magnetic flux density (1 T). Thus, the use of the second mechanism may be advantageous in designing an actuator with large strain capability.

The third mechanism,[6,9] termed as "hybrid mechanism," is based on a set of chain reactions. An applied magnetic flux (or field) *gradient* induces magnetic force which causes stress induced martensite phase transformation resulting in the phase change from stiff austenite to soft martensite phase, thereby leading to large displacement. The advantages of this are large stress (100 MPa in the case of FePd), modest to intermediate strain, and fast actuation time. Physically, such a phase change can be achieved by approaching a compact and portable magnet close to the FSMA specimen which provides a large magnetic field gradient. Therefore, the third hybrid mechanism is considered most suited for use in designing compact actuators with large force capability.

However, the cost of processing FSMAs such as FePd is very expensive. On the other hand, superelastic shape memory alloys have high mechanical performances and large transformation strain and stress capabilities. However, the speed of superelastic SMAs by changing *temperature* is slow. If a ferromagnetic shape memory alloy composite composed of a ferromagnetic material (soft magnet) and a superelastic SMA can be developed and such a composite be actuated based on the hybrid mechanism, cost-effective and high-speed actuators can be designed. This has been the underlying motivation of the present work. In the design of such a composite, the requirements have been identified as follows: no plastic deformation of the ferromagnetic material and large transformation strain in superelastic SMA. In order to achieve the optimum microstructure of FSMA composites for actuator design, numerical models such as FEM or an analytical approach needs to be developed. Such an analytical model for FSMA composites with the aim of optimizing the microstructure of FSMA composite with emphasis on

[a]Electronic mail: sushasini@u.washington.edu
[b]Electronic mail: tayam@u.washington.edu

laminated composite and helical shaped composite has been developed earlier.[10]

This paper reports the analytical modeling of the magnetic properties of FSMA particulate composites and also elucidates the experimental work of processing such composites. The validity of the proposed model has been established by comparison with the measured magnetic properties of the composite.

This paper has been organized as follows. The processing of particulate Fe–TiNi composite using spark plasma sintering (SPS) with various concentrations of Fe will be discussed in Sec. II, followed by the analytical model for predicting the effective magnetic properties of the particulate composites in Sec. III. A brief discussion of the results and validity of the proposed model will be presented in Sec. IV, followed by some conclusions in Sec. V.

PROCESSING OF PARTICULATE Fe–TiNi COMPOSITE

The FSMA composite used in the present work is a "particulate composite" composed of particulate powders of SMA (TiNi) and ferromagnetic material (soft magnetic Fe). The ordinary metallurgical route for processing particulate composites using powders, i.e., standard sintering, produces unwanted reaction products, destroying the original properties of the constituent SMA and ferromagnet. In order to circumvent unwanted reaction by-products, SPS machine was used to process the particulate composites. The SPS machine has been recently installed at the Center for Intelligent Materials and Systems (CIMS), University of Washington, Seattle (Dr. Sinter SPS-515S, Sumitomo Coal Mining Co., Japan). Figure 1 is a schematic of the SPS equipment and the sintering process.[11] It has been reported that sintering conducted using the SPS machine under high temperatures and pressure of around 25–50 MPa for as short a time as 5 min in near vacuum conditions (~5–6 Pa) followed by rapid cooling using argon gas produces remarkably good results.[12] In fact, as shown earlier, due to the short sintering time, the samples produced at CIMS were of extremely high quality, exhibiting low percentage of the intermetallics.[13]

In this study, two different kinds of TiNi powders have been used, namely, (1) large microsized TiNi (50.9 at. % Ni and 49.1 at. % Ti) with average diameter of 212 μm supplied by Sumitomo Metals, Japan, and (2) smaller nanosized TiNi (51 at. % Ni and 49 at. % Ti) with average diameter of 100 nm supplied by Argonide, USA. An ingot of TiNi alloy made by Sumitomo Metals, Osaka, Japan, was shipped to Fukuda Metals, Kyoto, Japan, where plasma rotating electrode process (PREP) was used to process TiNi powders with average diameter of 212 μm. The particulate FSMA composite specimens obtained using these powders were analyzed for superelastic properties. The results would be presented at a later point.

Iron metal powders of average particle size of 100 nm were purchased from Argonide Inc. These were processed by electroexplosion wire (EEW) technique. The chemical composition of the iron wire (soft iron) used by Argonide to make the metal powders is as follows: 0.78%–0.82% Mn, <0.1% Cr, 0.08%–0.098% Ni, 0.66%–0.82% Si, 0.081%–0.082% Cu, <0.05% V, <0.01% Mo, <0.1% W, and carbon whose content was not determined.

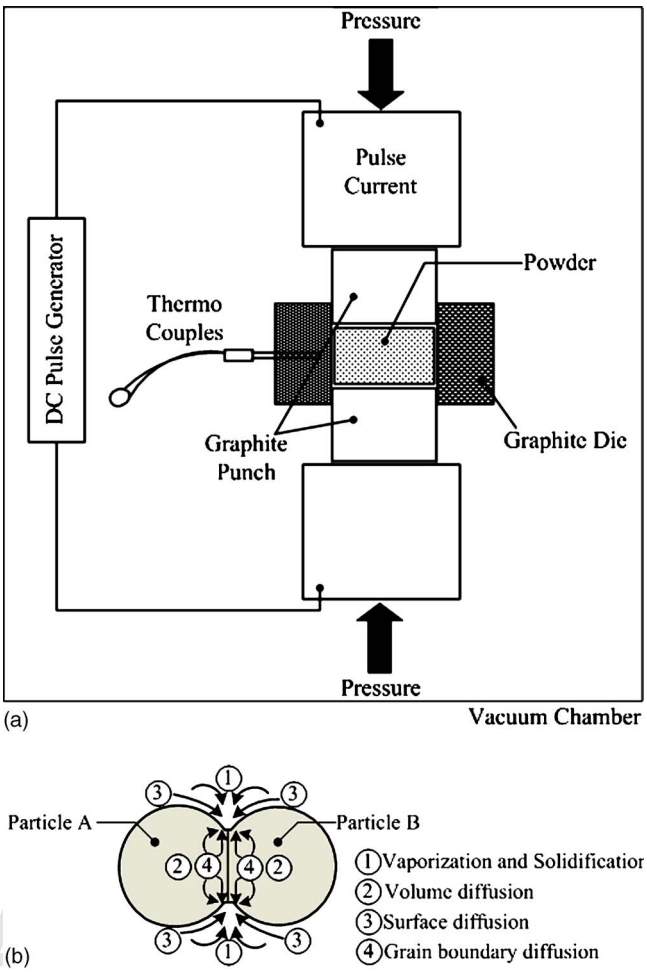

FIG. 1. Schematic of (a) SPS device and (b) SPS process (Ref. 13).

Due to the very small particle size (100 nm), these iron powders are very reactive and special care was taken while handling them. They were stored in vacuum sealed glass vials in a dormant state mixed with hexane. The required weight fractions of iron powder and TiNi powder were taken in a glass vial and acetylene solution was added to it. The glass vial was then put in a Thinky® mixer for 10 min to obtain a homogeneous mixture of the powders on evaporation of acetylene. The presence of acetylene not only aided the mixing process but also prevented the iron powder from getting oxidized. The homogeneous mixture was then placed in the mold and sintering operation was conducted at the set temperature, heating rate, and pressure. After sintering, each sample was aged at 320 °C for 30 min. This aging condition was chosen based on our previous results documented by Zhao *et al.*[19]

The results of the SPS processing of TiNi–Fe composites are summarized in Table I. It was not possible to obtain dense samples exhibiting superelasticity using nanosized TiNi and Fe powders. The SPS processing of pure TiNi samples using the nanosized TiNi powders under 900 °C and 50 MPa resulted in a high density TiNi specimen with its porosity reduced to 2%. However, differential scanning calo-

TABLE I. Summary of SPS processed TiNi–Fe composites including 100% TiNi specimen.

	Sample ID SPS conditions, composition	Density measured (g/cm^3)	Theoretical density (g/cm^3)	Porosity (%)
Nanosized TiNi powder	600 °C×5 min×50 MPa, 100 K/min pure 51 at. % TiNi (100 nm) sample	4.16	6.40	35
	800 °C×5 min×50 MPa, 100 K/min pure 51 at. % TiNi (100 nm) sample	4.90	6.40	23.4
	850 °C×5 min×50 MPa, 100 K/min pure 51 at. % TiNi (100 nm) sample	5.55	6.40	13.3
	900 °C×5 min×50 MPa, 100 K/min pure 51 at. % TiNi (100 nm) sample	6.27	6.40	2.0
Microsized TiNi powder	600 °C×5 min×50 MPa, 100 K/min 51 at. % TiNi (212 μm)+33.33 wt % Fe (100 nm)	6.66	6.88	3.2
	700 °C×5 min×50 MPa, 100 K/min 51 at. % TiNi (212 μm)+33.33 wt % Fe (100 nm)	6.65	6.88	3.2
	800 °C×5 min×50 MPa, 100 K/min 51 at. % TiNi (212 μm)+33.33 wt % Fe (100 nm)	6.65	6.88	3.2
	700 °C×5 min×50 MPa, 100 K/min 51 at. % TiNi (212 μm)+33.33 wt % Fe (74 μm)	6.56	6.88	4.6
	900 °C×5 min×50 MPa, 100 K/min pure 51 at. % TiNi (212 μm) sample	6.26	6.40	2.1

rimeter (DSC) (Perkin Elmer DSC-6) data of this TiNi specimen did not exhibit any shape memory properties. In fact, x-ray diffraction (XRD) results of this TiNi specimen showed $TiNi_3$ peaks which persisted after solution quenching (see Fig. 2).[15] These poor data of TiNi–Fe composite using nanosized TiNi powders led us to switch to larger microsized TiNi powers and nanosized Fe powders.

The results of SPS processed composites using this combination is shown in the lower half of Table I where relative densities of 97% and higher were obtained at reasonably low sintering temperatures of around 700 °C. The iron particles fill in the gaps between TiNi powders and form the matrix phase of the composite after the sintering operation is completed. The microstructures of these sintered samples

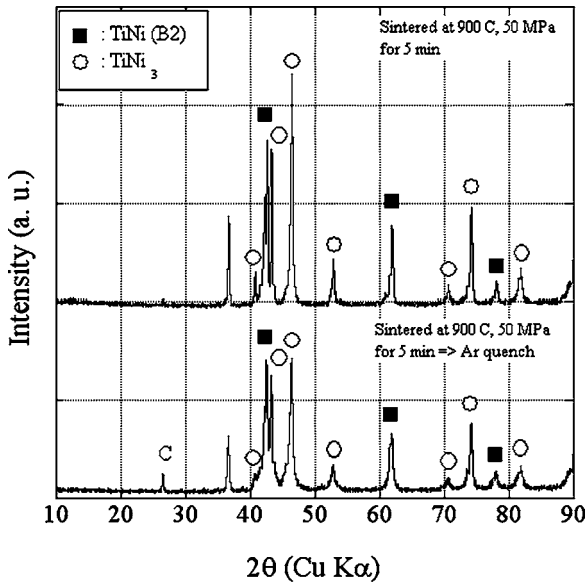

FIG. 2. XRD data of 900 °C×5 min×50 MPa, 100 K/min pure 51 at. % TiNi (100 nm) sample.

(700 °C SPS) are characterized using scanning electron microscopy (SEM) (T330A Hitachi). Figure 3 shows SEM images of a finely polished specimen after sintering. Structural compositions of the samples are characterized using XRD. The density is measured using a technique based on Archimede's principle.

Determination of the transformation temperatures was the next step in the material characterization process. This was conducted by DSC tests with a heating/cooling rate of 10 °C. DSC experiments of the dense SPS specimen of 30 wt % TiNi (212 μm diameter)+70 wt % Fe (100 nm) processed at 700 °C, 5 min sintering time, and 50 MPa pressure revealed the transformation temperatures as A_f (austenite finish)=40°C, A_s (austenite start)=28°C, M_f (martensite finish)=15°C, and M_s (martensite start)=30°C. These TiNi–Fe composite specimens were then cut into cylinders of 5 mm diameter using electrical discharge machining (EDM). The specimens were then tested using Instron model 8562 compression testing equipment. Figure 4(b) depicts a typical stress-strain response of TiNi–Fe composite tested at 41 °C (which is slightly higher than A_f=40 °C) exhibiting a superelastic loop.

THEORETICAL MODEL

Composite magnetic permeability

In this section, Eshelby's equivalent inclusion method[16] in conjunction with Mori-Tanaka's mean-field theory[17] has been used to predict the effective magnetic properties (effective magnetic permeability and saturation magnetization) of Fe–TiNi particulate composite. The first step involved defining a representative volume element (RVE) of the particulate composite used in this study. To this end, the Fe phase was chosen as the f phase or inhomogeneity and the TiNi SMA phase was chosen as the m phase in the RVE, as depicted in Fig. 5. The implications of such a definition will be discussed

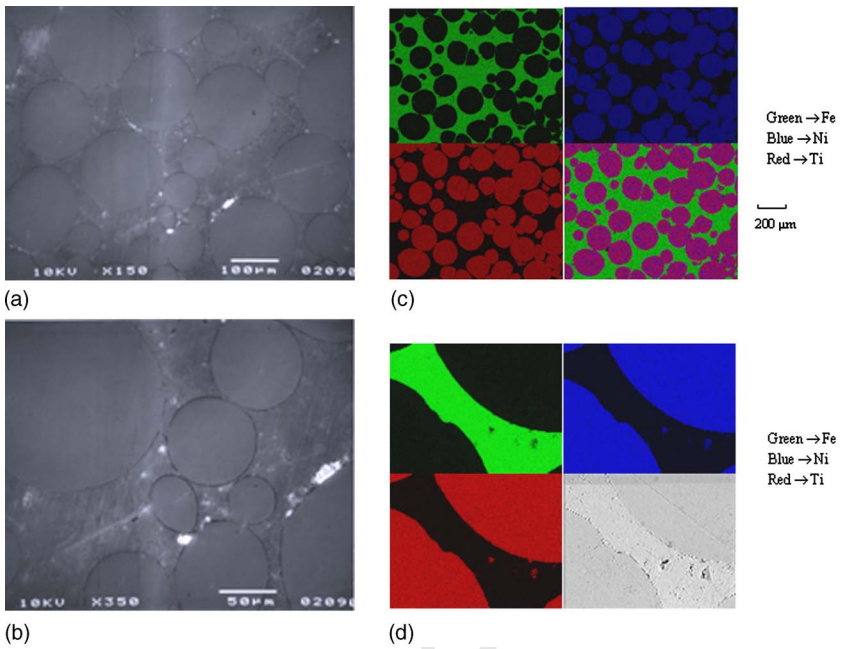

FIG. 3. SEM images of the processed 33.33 wt % Fe (100 nm)+66.67 wt %, 51 at. % TiNi (212 μm) particulate composite. (a) 150× magnification image, (b) 350× magnification image, (c) area composition map, and (d) line compositional map.

at a later point. Thus, the properties of the Fe phase are represented by the subscript f in the evolution of Eshelby's model while the properties of SMA are denoted by the subscript m, as depicted in Fig. 5. In the absence of inhomogeneities, the matrix SMA phase has the following property:

$$B = \mu_m \cdot H_m, \tag{1}$$

where B is the magnetic flux, H_m is the magnetic field intensity, and μ_m is the magnetic permeability of the matrix material. Equation (1) is reminiscent of an originally proposed equivalent stress-strain formulation and now widely accepted Eshelby model.[16] For paramagnetic materials (such as TiNi SMA material), the magnetic susceptibility χ typically lies in the range of $10^{-3}-10^{-5}$; consequently, the magnetization vector is very weak. Therefore, the magnetic field intensity in the matrix phase takes the following form:[18]

$$H_m = H_o + M \Leftrightarrow H_m \approx H_o, \tag{2}$$

where H_o is the applied magnetic field intensity on the domain under consideration as depicted in Fig. 5(a). Essentially, Eq. (2) conveys that due to the weak magnetization of paramagnetic materials constituting the particulate phase of the composite domain, the magnetic field intensity of the matrix phase would be equal to the applied magnetic field intensity. Equation (2) is valid for most paramagnetic materials such as TiNi for which the magnetization vector $M \approx 0$. Equation (1) can thus be written as

$$B = \mu_m \cdot H_o. \tag{3}$$

The error associated with neglecting the magnetization for paramagnetics has been found to be of the order of 0.01%, which is considered acceptable in the present work.[18] Upon addition of an inhomogeneity (f phase), the flux and field vectors are related as follows in Ω (see Fig. 5):

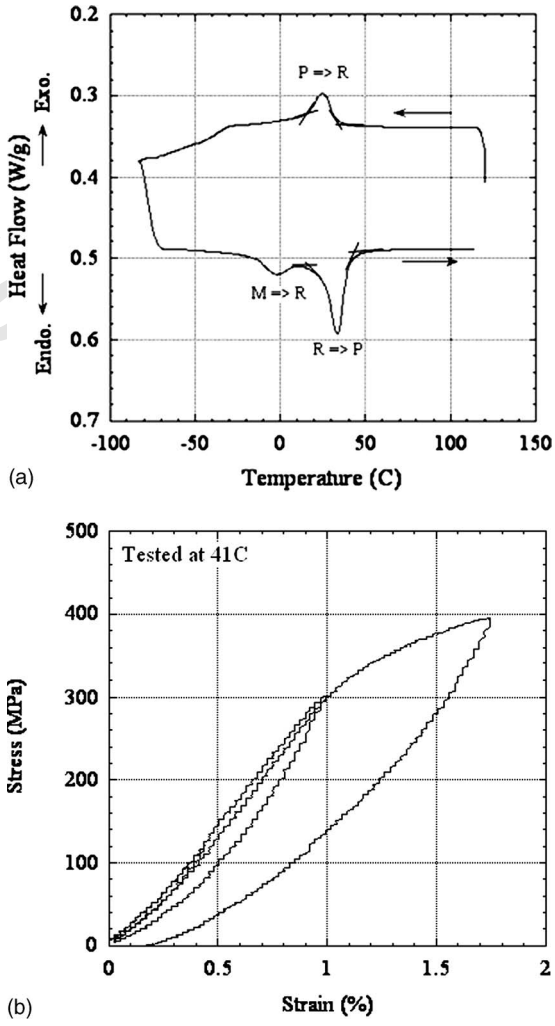

FIG. 4. TiNi 30 wt % Fe composite specimen with SPS at 700 °C, 5 min, 50 MPa pressure, then aged at 320 °C for 1 h experimental results. (a) DSC data yielding A_f=40 °C, A_s=28 °C, M_s=30 °C, and M_f=15 °C. (b) Compression stress-strain curve of this composite specimen at 41 °C (=A_f), exhibiting to some extent superelastic loop.

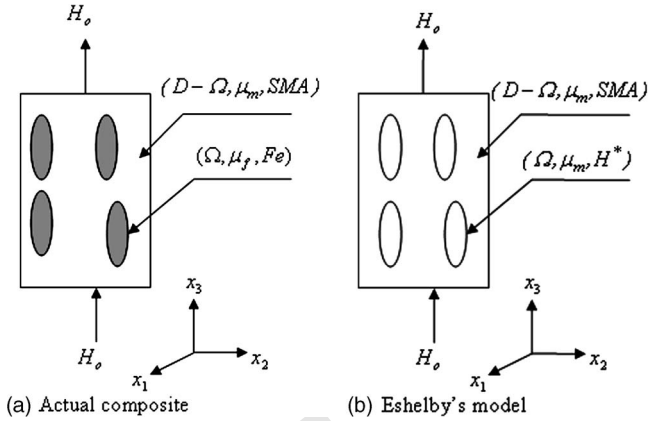

FIG. 5. Analytical modeling of particulate TiNi–Fe composite based on Eshelby's equivalent inclusion method. (a) Schematic of the actual composite and (b) Eshelby's model.

$$B + B_d = \mu_f \cdot (H_o + H_d) = \mu_m \cdot (H_o + H_d - H^*), \quad (4)$$

where B_d and H_d are the disturbance flux and field vectors, respectively. Physically, H_d represents the demagnetization field characteristic of ferromagnetics. By definition for ferromagnetics,

$$B = \mu_o \cdot (H_o + M - N \cdot M) = \mu_f \cdot (H - N \cdot M), \quad (5)$$

where N is the demagnetization factor, a tensor quantity depending only on the shape of the inhomogeneity, analogous to Eshelby's tensor S of the mechanical case. Choosing $H_d = -N \cdot M$ in Eq. (5), we get

$$H_d = N \cdot H^* = S^m \cdot H^* \quad \text{or } B + B_d = \mu_f \cdot (H_o + S^m \cdot H^*) = \mu_m \cdot (H_o + S^m \cdot H^* - H^*), \quad (6)$$

where $S^m = N$ has been looked upon as the "Eshelby tensor" for the magnetic case. From Eq. (6), H^* can be solved. When the volume fraction of ferromagnetic inhomogeneities (f) becomes finite, the interactions between ferromagnetic particles need to be accounted for. This has been accomplished by utilizing Mori-Tanaka's mean-field theory in the present case (atomic interaction effects have been neglected here). $\bar{H}$ has been coined as the average magnetic field and Eq. (6) is modified as follows taking into account the volume fraction effects:

$$B + B_d = \mu_f \cdot (H_o + \bar{H} + H_d) = \mu_m \cdot (H_o + \bar{H} + H_d - H^*) \quad \text{or } B_d = \mu_m \cdot (\bar{H} + H_d - H^*). \quad (7)$$

Since the volume integration of H_d must vanish over the entire domain, we get

$$\bar{H} = -f(H_d - H^*). \quad (8)$$

Substituting in (7) and simplifying gives us

$$H^* = \{(\mu_f - \mu_m) \cdot [(1-f)S^m + fI] + \mu_m\}^{-1} \cdot (\mu_m - \mu_f) \cdot H_o. \quad (9)$$

The corresponding concentration factor tensor A can be evaluated as[16]

$$H_f = H_o + \bar{H} + H_d = H_o + H_d(1-f) + fH^* = H_o + [(1-f)S^m + fI] \cdot H^* \quad \text{or } H_f = A \cdot H_o, \quad (10)$$

with

$$A = (I + [(1-f)S^m + fI] \cdot \{(\mu_f - \mu_m) \cdot [(1-f)S^m + fI] + \mu_m\}^{-1} \cdot (\mu_m - \mu_f)).$$

Therefore,

$$\mu_c = \mu_m + f(\mu_f - \mu_m) \cdot A, \quad (11)$$

where μ_c represents the effective magnetic permeability of the composite. Therefore, by knowing the properties of the individual constituents of the composite and the geometry of the inclusion, the composite magnetic permeability can be evaluated. The computation of the demagnetization factor has been done by many researchers and the values are therefore known.[19,20]

Saturation magnetization (M_s^c)

The magnetic field intensity in the composite is evaluated as follows:

$$H_c = (1-f)\langle H_m \rangle + f\langle H_f \rangle,$$

where $\langle H_m \rangle$, $\langle H_f \rangle$ are volume averaged quantities (the angular brackets denote volume average over the entire domain). Using the procedure outlined in Taya's book,[21] the composite magnetic field intensity takes the following form:

$$H_c = H_o + M_s^c = H_o + fM_s \quad \text{or } M_s^c = fM_s. \quad (12)$$

Here, M_s is the saturation magnetization of the ferroparticulate or the f phase of the composite and M_s^c represents the composite saturation magnetization. Based on this formulation, the magnetization at saturation M_s of TiNi–Fe composites processed at different weight fractions was predicted and compared with the experimental values. The following section outlines the results.

RESULTS

After characterizing the sintered samples with various volume fractions as shown in Table I, the samples satisfying the key requirements (DSC showing peaks of shape memory properties) were chosen, namely, particulate TiNi/Fe processed by SPS at 700 °C in vacuum for 5 min and 50 MPa with 30%, 50% and 70% Fe by weight. The magnetization (**M**)–magnetic field (**H**) curves of the composite specimens were then measured using the vibrating specimen magnetometer (VSM) located at Tohoku University in order to compare with the theoretical predictions. The model predictions of saturation magnetization were compared with measured magnetization at saturation, resulting in a good match. A comparison of magnetization at saturation (M_s) of TiNi–Fe composites between predictions and experimental data is summarized in Table II.

The results of Table II have also been plotted in Fig. 6. Table II and Fig. 6 show good agreement between the experiment and the proposed analytical model despite the fact that at lower wt % of Fe filler, the predicted M_s^c is slightly

TABLE II. Comparison of predicted magnetization at saturation of TiNi–Fe particulate with measured data.

Fe (wt. %)	Volume fraction of Fe[a] (f)	M_s^c (emu/g) Expt.	M_s^c (emu/g) Predicted
30	0.26133	40	52.266
50	0.4522	93	90.44
70	0.6582	135	131.64
100	1.0	200	200

[a] $f=\{1/1+[(1-w)/w]\rho_{Fe}/\rho_{NiTi}\}$; ρ_{Fe}, ρ_{NiTi} are the densities of Fe and TiNi (7874 and 6500 g/cm^3, respectively).

overestimated. At lower f, smaller sized Fe particles tend to be distributed along the boundaries of larger sized NiTi particles.[13] At larger f, on the other hand, Fe filler particles become more uniformly distributed, forming a continuous matrix, similar to the model configuration [Fig. 5(a)]. Therefore, for lower f, the predicted values of M_s^c deviate slightly from the experimental data while for larger f, we see very good agreement, as evidenced in Table II and Fig. 6.

The present model is based on Eshelby's effective medium theory (EMT) with Mori-Tanaka's mean-field theory; thus its validity is good for the entire range of filler weight (volume) fraction, $0 \leqslant f \leqslant 1$. It should further be pointed out here that the average size of NiTi is 212 μm, which is considerably larger than that of the constituent Fe powder of 100 nm size. Compositional maps of the particulate composites indicated that the Fe phase forms the matrix phase of the composite unlike the model presented in Fig. 5. The implications of this discrepancy need to be investigated further and shall be looked into in future studies. However, despite this assumption, as mentioned previously, the predictions seem to match with the observed experimental values.

CONCLUSIONS

The combination of microsized TiNi powders and nanosized Fe powders resulted in the formation of high density specimens which exhibited superior stress-strain characteristics. Nanosized Fe powders tend to fill in the gaps between microsized TiNi powders much better than microsized Fe powders, thereby enhancing the bonding, resulting in stronger load transference at TiNi–Fe interfaces. Such an interface behavior facilitates the phase transformation demonstrated by the TiNi phase of the composite. This synergy between the two phases of the composite is expected to benefit actuator designers using this particular material system. Several combinations of the microsized TiNi and nanosized Fe were chosen and the respective stress-strain curves for each combination were looked upon. Due to obvious space constraints, not all the stress-strain curves have been included in this paper. Instead, one representative stress-strain curve demonstrating the phase transformation phenomenon has been included in the present work. The selection of an optimal volume fraction of TiNi and temperature/pressure/duration of SPS process was found to be very critical in the formation of a sample that would exhibit the SMA properties under compression testing.[22] Consequently, series of experiments were conducted to identify these optimal volume fraction and SPS process conditions using a design of experiments approach and a few optimal conditions have been identified. The microstructure of the composite was also studied using SEM and transmission electron microscopy (TEM) studies.

An extension of Eshelby's method for the determination of effective magnetic properties of a FSMA system has been proposed in the present paper and the predicted results were compared with experimental results, leading to a validation of the proposed model.

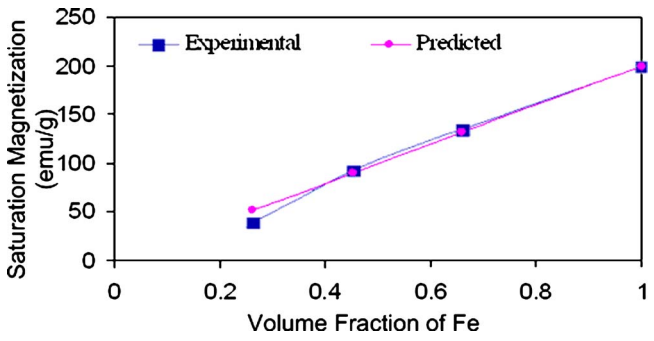

FIG. 6. Comparison of saturation magnetization (M_s) of TiNi–Fe particulate composites as a function of Fe predicted by Eshelby's model (filled circular symbols) and experimental data (filled square symbols).

ACKNOWLEDGMENTS

Two of the authors (S.G. and M.T.) are thankful to the U.S. AFOSR (F49620-02-1-0028) for supporting the present analytical study where Dr. B. S. (Les) Lee is the program manager. The authors are thankful to Kise of Sumitomo Metals for providing high quality TiNi powders of superelastic grade and also to Leonid Kaledin of Argonide Inc. for providing soft Fe powders.

[1] K. Ullakko, J. K. Hung, V. V. Kokorin, and R. C. O'Handley, Scr. Mater. **36**, 1133 (1997).
[2] R. D. James and M. Wuttig, Philos. Mag. A **77**, 1273 (1998).
[3] S. J. Murray, M. Frinelli, C. Kanter, J. K. Hung, S. M. Allen, and R. C. O'Handley, J. Appl. Phys. **83**, 7297 (1998).
[4] T. Kakeshita, T. Takeuchi, T. Fukuda, M. Tsujiguchi, T. Saburi, and R. Oshima, Appl. Phys. Lett. **77**, 1502 (2000).
[5] Y. Liang, H. Kato, M. Taya, and T. Mori, Scr. Mater. **45**, 569 (2001).
[6] H. Kato, T. Wada, Y. Liang, T. Tagawa, M. Taya, and T. Mori, Mater. Sci. Eng., A **332**, 134 (2002).
[7] Y. Liang, T. Wada, H. Kato, T. Tagawa, M. Taya, and T. Mori, Mater. Sci. Eng., A **338**, 89 (2002).
[8] T. Wada, Y. Liang, H. Kato, T. Tagawa, M. Taya, and T. Mori, Mater. Sci. Eng., A **361**, 75 (2003).
[9] Y. Liang and M. Taya, Mech. Mater. **38**, 564 (2006).
[10] M. Kusaka and M. Taya, J. Compos. Mater. **38**, 1011 (2004).
[11] SPS Syntex Inc. manual (http://www.scm-sps.com/; last accessed: 20 February 2007).
[12] S. Gururaja, H. Nakayama, and M. Taya, Proc. SPIE **6170**, 617018 (2006).
[13] S. Gururaja, M. Taya, H. Nakayama, Y. S. Kang, A. Kawasaki, and Y. Sutou, Proc. SPIE **4761**, 548 (2005).
[14] Y. Zhao, M. Taya, Y. Kang, and A. Kawasaki, Acta Mater. **53**, 337 (2005).
[15] J. K. Allafi, A. Dlouhy, and G. Eggeler, J. Phys. IV **212**, 681 (2003).
[16] J. D. Eshelby, Philos. Trans. R. Soc. London, Ser. A **241**, 516 (1957).
[17] T. Mori and K. Tanaka, Acta Metall. **21**, 571 (1973).
[18] S. Chikazumi, *Physics of Magnetism* (Wiley, New York, 1964).
[19] M. Beleggia and M. De Graef, J. Magn. Magn. Mater. **263**, L1-9 (2003).
[20] J. A. Osborn, Phys. Rev. **67**, 351 (1945).
[21] M. Taya, *Electronic Composites: Modeling, Characterization, Processing, and MEMS Applications* (Cambridge University Press, Cambridge, 2005).
[22] V. Mamedov, Powder Metall. **45**, 322 (2002).

AQ: #8

AUTHOR QUERIES — 035717JAP

#1 Author-Please supply zipcode for Japan address
#2 Author-Please note that JAP does not allow claims of novely Pls. check deletion
#3 Author-Please define “FEM”
#4 Author-refs. were not cited in numerical order. Pls. check renumbering
#5 Author-“%wt” changed to “wt%” throughout. Pls. confirm
#6 Author-footnotes in text are not allowed. Pls. check incorporation in text throughout
#7 Author-Please note that you had no Eq. 10. Pls. check renumbering
#8 Author-Ref. 22 was not cited in text. Pls. check insertion